Benchmarking of hysteretic elements in topological transformer model

H. K. Høidalen, A. Lotfi, S. E. Zirka, Y. I. Moroz, N. Chiesa, and B. A. Mork

***Abstract*—Transformer core modeling is of importance for some transient studies like inrush currents, ferroresonance and geomagnetically induced current. This paper compares a transformer model with different magnetization representations to actual measurements. Piecewise nonlinear (Type 98) or hysteretic inductors (Type 96) both in parallel to a constant resistance, Jiles-Atherton hysteretic inductance and a newly developed inverse dynamic hysteresis model (DHM) are tested for open circuit response, residual flux after switching out, and inrush currents when energizing the transformer. The models have all problems of reproducing the magnetization current waveforms and there are substantial differences between the models in residual flux estimation resulting in quite different inrush patterns. The DHM model is the easiest to use as few parameters are required and the model gives fairly well agreement with measurements.**

***Keywords*: Transformer, hysteresis, test report, residual flux, inrush current.**

I. Introduction

TOPOLOGICAL transformer models are important to accurately predict steady-state regimes and transient behaviors, from steady-state losses to inrush currents [1, 2]. Shortcomings of available models are primarily in the imperfection of the core model and in particular in the estimation of frequency dependency, nonlinear losses and residual flux. This is important for studying ferroresonance, inrush currents, and geomagnetically induced currents.

Previously, the Hybrid Transformer model was presented at IPST [3, 4] and this model extends the classical BCTRAN model [5] with a topological core with fitting to open circuit test report data. The core equivalent in this model is represented by nonlinear inductances (Type 98) in parallel to constant core-loss resistances. The model has also an option to use a hysteretic inductance (Type 96) representing a part of the total core loss [6, 7]. In attempts to better reproduce residual flux, the model was extended with a Jiles-Atherton (JA) hysteresis model [8-10]. The JA model is not publicly available and the parameter determination procedure is complicated.

Recently, a new dynamic hysteresis model (DHM) has been implemented in the ATP-EMTP [13]. This three-component DHM consists of a static hysteresis model (SHM) [11] implemented as a rate-independent hysteretic inductor, and two resistive elements, linear and nonlinear, reproducing classical eddy-current and excess losses respectively. This model is based on steel manufacturer's data including static hysteresis loops, catalog losses and the DC magnetization curve reaching induction levels with differential permeability μ_0. When the DHM is incorporated into a transformer model, the presupposed or manufacturer provided core geometry and turn numbers are employed to recalculate magnetic variables (the magnetic field H and induction B) into flux-current curves of the legs and yokes. Although the DHM itself has shown performance in agreement with Epstein frame measurements [12], the model should always be fitted to the no-load test of a specific transformer. This is due to uncertainties in the stacking factor and joint air gaps as well as increased losses in real designs compared to catalog data.

Section II gives the transformer test report and design data, section III outlines the transformer model used, and Section IV compares simulations and measurements.

II. Transformer Data

A 300 kVA Yyn-connected distribution transformer is used as test object for the benchmarking. The test report is given in Table I, both for open and short circuit tests. Both true rms and average rectified voltage scaled to rms are reported in the table. There are significant differences between the two voltages above 100% excitation indicating high waveform distortions. The V_{ARV} is used in the rest of this paper as it gives a better representation of the peak flux.

TABLE I Transformer Test Report

OC test.	V (rms),%	V (ARV),%	I_0,%	P_0, kW
Voltage on LV Side	80.803	80.550	0.2749	0.3531
	90.033	89.580	0.4047	0.4548
	94.255	93.620	0.5006	0.5118
	97.518	96.670	0.6000	0.5625
	101.540	100.240	0.7800	0.6352
	108.910	105.990	1.4927	0.7936
	113.090	108.830	2.3205	0.8917
	116.456	111.030	3.4029	0.9786
	118.409	112.280	4.2701	1.0359
	120.595	113.600	5.5446	1.1094
	127.731	116.790	15.2612	1.5562
SC test	[kV]	[kVA]	V_{SC}[%]	P_{SC} [kW]
HS/LS	11.43/0.235	300	4.1	3.187

This work received financial support from the EM-Transients project at SINTEF Energy Research and the Norwegian Research Council.

H. K. Høidalen and A. Lotfi are with the Norwegian University of Science and Technology, Trondheim, Norway (hans.hoidalen@elkraft.ntnu.no).

S. E. Zirka and Y. I. Moroz are with the Department of Physics and Technology, Dnepropetrovsk National University, Dnepropetrovsk, Ukraine 49050 (zirka@email.dp.ua).

N. Chiesa is with Statoil, Norway (NCHIE@statoil.com) and B.A. Mork is with Michigan Technological University, USA (bamork@mtu.edu).

Paper submitted to the International Conference on Power Systems Transients (IPST2015) in Cavtat, Croatia June 15-18, 2015

Transformer core dimensions are given in Table II where the cross sections of the legs and yokes were determined from geometrical dimensions of their packs (the stacking factor (SF) of 1.0 was supposed). The 3-legged core is stacked with the Armco 0.3-mm thick steel M5 with resistivity of 0.48 μΩ·m. A stacking factor of 0.965 is later assumed for the DHM model. The number of turns in the star-connected LV windings is 21.

TABLE II
CORE DIMENSIONS

Core part	Area [mm^2]	Length [mm]
Leg	17528	670
Yoke	19812	580

III. TRANSFORMER MODEL

A simple, but topologically correct transformer model is used to benchmark the influence of various magnetization branch representations. Fig. 1 shows the basic structure of the transformer model for a 3-legged core. The model is somewhat modified compared to the Hybrid Transformer model [3-4] as the magnetization branch of the legs more correctly is connected to the opposite side of the leakage inductance. This difference in leg connection is found to have little influence [9]. The leakage model is based on only two inductances L_{LC} and L_{HL}, plus the zero-sequence inductance. The inductances and resistance are split in two halves to obtain symmetry. In addition to the core and winding parts shown in Fig. 1, capacitances are added to the terminals of the LV and HV windings.

A. Transformer model quantities

Based on the test report in Table I, the parameters of the model in Fig. 1 are calculated. The leakage inductance is

$$L_{HL} = \sqrt{\left(\frac{e_k}{100}\right)^2 - \left(P_k / S\right)^2} \cdot \frac{V_L^2}{S} \cdot \frac{1}{2\pi f} = 23.2\ \mu\text{H}. \qquad (1)$$

The off-core inductance between the LV winding and the core, L_{LC} is assumed to be 0.33 of the leakage inductance. This can be estimated from the winding design information and is approximately the ratio between the distance from the LV winding to the core and the distance between the LV and HV windings. A factor of 0.5 is used in the Hybrid Transformer model [3]. The frequency is 50 Hz.

The final slope of the magnetization inductance of the leg is estimated from the design information;

$$L_\infty = \mu_0 \cdot N^2 \cdot A_L / l_L = 14.5\ \mu\text{H}. \qquad (2)$$

The winding resistance is

$$R_{LH} = \frac{P_k}{S} \cdot \frac{V_L^2}{S} = 1.9556\ \text{m}\Omega. \qquad (3)$$

This is split between the LV and HV side based on the measures DC resistance ratio (61.6% on the LV side) so that

$$R_L = R_{LH} \cdot 0.616 = 1.2054\ \text{m}\Omega \qquad (4)$$

$$R_L = R_{LH} \cdot 0.384 \cdot \frac{V_H^2}{V_L^2} = 1.7747\ \Omega \qquad (5)$$

The zero-sequence impedance is measured separately as L_0=0.42 mH. This value is of little significance in the no-load from the LV terminals, but has some influence on the inrush currents calculated for HV excitations.

The capacitances are also measured as C_L=1.115 nF, C_{HL}=0.495 nF, C_{Hac}=0.236 nF, C_{Hb}=0.163 nF. In addition, there is a 0.2 nF added to the HV side to represent the voltage divider. These capacitances have some relevance for the ring-down transients only, but are kept to ease numerical complications due to the isolated neutral on the HV side.

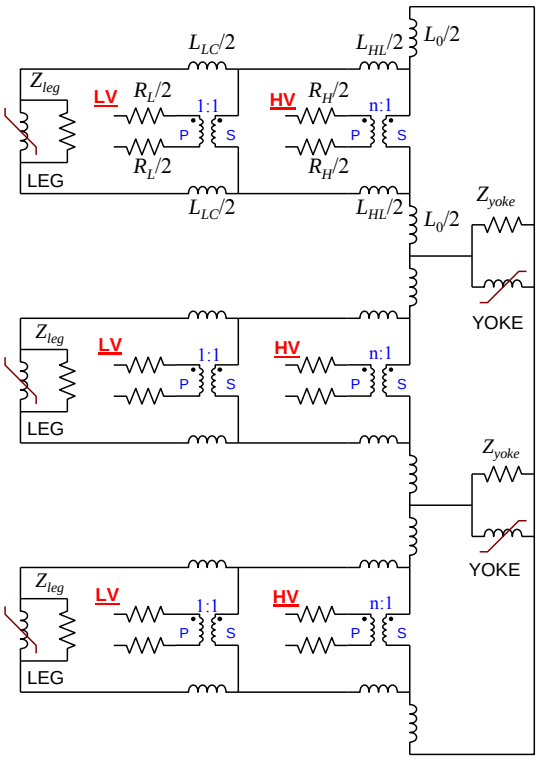

Fig. 1. Electric model of the transformer [4], 2-windings (HV and LV), 3-phases, 3-legged core.

B. Magnetization models

In Fig. 1, the impedances marked as Z_{leg} and Z_{yoke} for the leg and yoke respectively will be subjected to change. The following magnetization models will be benchmarked:

1) Type 98.

Piecewise nonlinear inductance with core loss modeled with a constant resistance in parallel (eddy current model). The nonlinear inductance is assumed to follow a modified Frolich equation [10]

$$\lambda(i) / A_r = \frac{i / l_r}{a + b \cdot |i| / l_r + c \cdot \sqrt{|i| / l_r}} + L_\infty \cdot i / l_r \qquad (6)$$

The constants a, b, c in (6) are fitted to the magnetization current in the open circuit test report and the resistance is fitted to the core loss at 100% excitation. The Hybrid Transformer model [3, 4] is in practice used to obtain the numerical values. The final slope L_∞ is found from (2).

2) Type 96.

Piecewise hysteretic inductance with half of the losses embedded in the hysteresis loop and the rest in a parallel

resistor [4]. The anhysteretic curve is equal to that of the Type 98 nonlinear inductor with a constant width of the hysteresis loop.

3) Jiles-Atherton model.

Jiles-Atherton model with all losses embedded in the dynamic hysteresis model is documented in [8, 9]. The fitting procedure is non-trivial for three-phase transformer models with a topological core model. Several instances of the JA module, one for each transformer limb, have to be solved together in a nonlinear and multidimensional optimization problem. It is reasonable to assume that the core material is the same and the total number of parameters does not multiply by the number of limbs, and the non-linear characteristic of each limb is scaled based on the relative cross-sectional area and length dimensions. The fitting of the parameters is done in two steps. First the parameters describing the anhysteretic magnetization curve are fitted to the peak flux-linkage/current values derived from open-circuit test report in a similar approach as for Type 98 above. It is assumed that the shape of the anhysteretic curve does not change as a function of frequency and magnetization level. The remaining parameters are then calculated with an optimization procedure to fit the losses to the open-circuit test-report. The traditional JA model only account for hysteresis losses. Rate dependent losses due to eddy current can be added to the model based on Bertotti's loss component splitting [14].

4) DHM.

Dynamic hysteresis model documented in [11]. The model requires the absolute leg/yoke dimensions, the number of LV turns and the choice of material from a predefined library. In addition comes three tuning factors, namely the stacking factor γ, loss factor K_{loss}, and a joint air-gap Δ. The stacking factor is multiplied to the leg and yoke area, while the loss factor K_{loss} is a parameter of the model and is multiplied to the eddy-current and anomalous fields. This results in the total loss $P = P_H + K_{loss} \cdot (P_E + P_A)$ where P_H, P_E, and P_A represent hysteresis, classical eddy current and excess loss components [14]. The joint air-gaps are modeled as an inductance in parallel with the leg model. The air-gap inductance is calculated according to (2) with l_L replaced by the air-gap Δ. For the basic DHM model the stacking and loss factors are set to unity and the air-gap to zero.

In addition, a fitted model is introduced called DHMfit where the stacking and loss factors are fitted to the test report data and the air-gap is adjusted to obtain the maximum measured residual flux. This resulted in γ=0.965, K_{loss}=1.3335 and an air-gap of 0.01 mm giving L_{ag}=937.4 mH.

IV. Results

This section compares simulation results for the five different magnetization models to measurements and test report quantities. First, the five basic magnetization models are compared. Then the full transformer model in Fig. 1 is used to benchmark for open circuit excitation, ring-down transients and inrush currents.

A. Core component test

Here the four base components described in Sect. III B are compared as shown in Fig. 2. The fluxlinkage-current characteristic at rated excitation is shown in Fig. 3. The basic DHM model has a too steep (catalog) hysteresis loop. When air-gap corrections are added the steepness is in agreement with the other three models all being relatively similar.

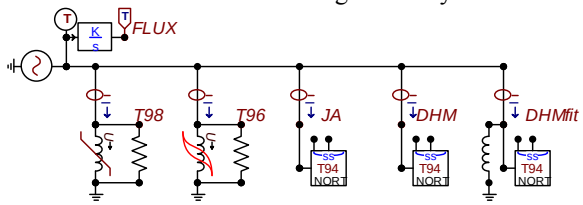

Fig. 2 Test configuration of the core base components

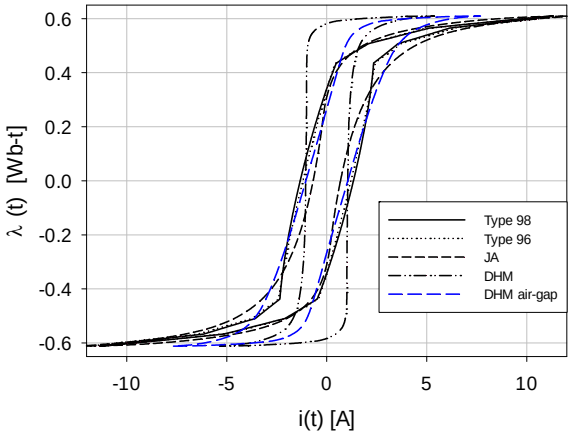

Fig. 3 Simulated hysteresis loops of the core base components.

B. Open circuit tests

The transformer model in Fig. 1 with the four different magnetization models are energized with sinusoidal voltage at the low-voltage side according to the test report voltages in Table I.

Fig. 4 shows the magnetization current in percent of rated current as a function of excitation voltage, while Fig. 5 shows the core loss in Watts.

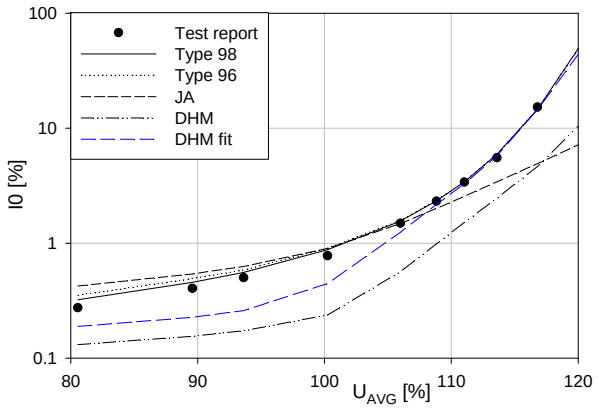

Fig. 4 Comparison of transformer model magnetization current with test report values.

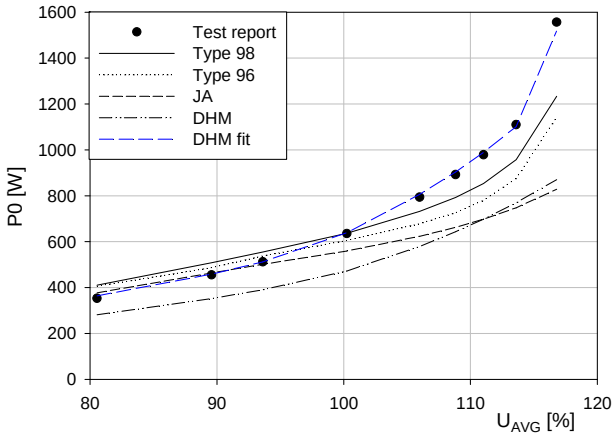

Fig. 5 Comparison of transformer model core loss with test report..

The Type 98 and Type 96 models are almost identical with a high agreement with the test report. This is expected as these two models are fitted directly to these data. The same applies to the JA-model. The DHM does not utilize the test report data so the lesser agreement is as expected. Adding the air-gap and K_{loss} corrections increases the magnetization current at low excitations.

Fig. 6 shows the shape of the magnetization current of the transformer in Fig. 1 compared to measurements for rated, sinusoidal excitation. None of the models are able to reproduce the measured large 3rd harmonic content of the magnetization current.

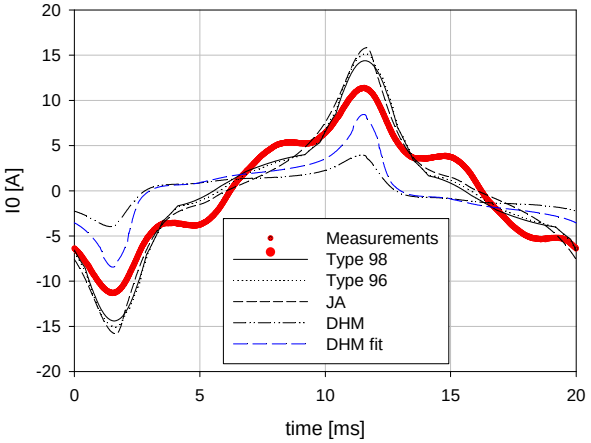

Fig. 6 Magnetization current shape compared to measurements at 100% excitation.

Fig. 7 shows the simulated and measured steady-state hysteresis loop seen from the LV side at rated excitations. The fluxlinkage is found by integrating the measured applied voltage. In the simulations the applied voltage is ideal and sinusoidal, while in the measurements some unbalance and harmonics (around 3% 5th harmonic) were observed as shown in Fig. 8. This real voltage shape and phase unbalance could have some influence on the magnetization current as the low zero sequence impedance starts to matter. There are significant differences in the fluxlinkage-magnetization current hysteresis loops for the three phases in the measurements as shown in Fig.8.

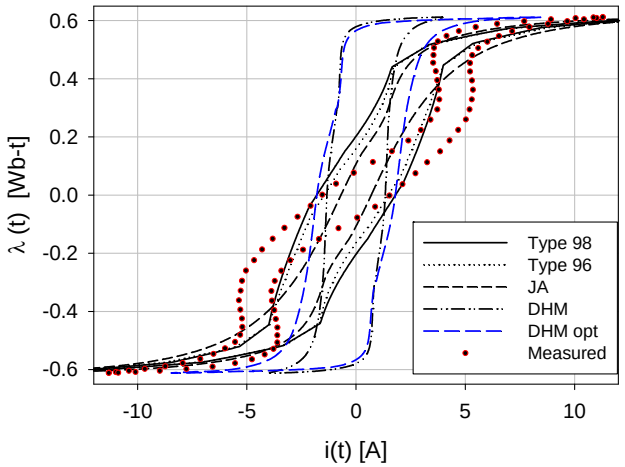

Fig. 7 Test of fluxlinkage-current characteristic phase A of transformer model in Fig. 1.

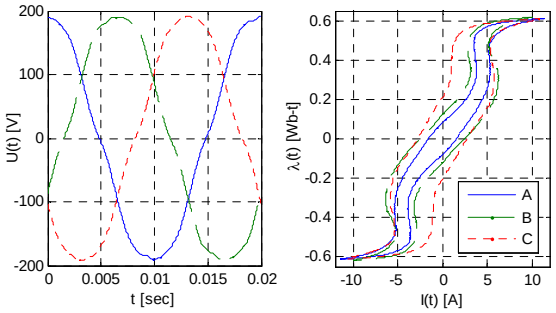

Fig. 8 Measured voltage (left) and fluxlinkage-magnetization loops (right) at rated excitation V_{avg}=100.24%.

C. *Ring-down tests*

In this test the unloaded transformer model in Fig. 1 is ramped up to steady state and then disconnected from the supply. A ring-down transient will occur where the capacitance of the transformer plays a significant role. Figs. 7 and 8 shows the simulated steady-state residual flux (after 0.2 sec.) as a function of switching out instance, where Δt_{open}=0 means at voltage peak phase A. Fig. 9 shows the result when the current is interrupted at zero crossing, while Fig. 10 shows the result when the current in all phases are chopped at the opening instance. One per unit fluxlinkage is 0.6107 [Wb-t].

Fig. 11 shows the measured residual flux as average of 20 measurements for each opening instance. The measured fluxlinkage (integral of measured induced voltage on the LV-side) follows a sinusoidal dependency of disconnection instance and is in agreement with the simulations where the current is chopped. The maximum measured residual fluxlinkage is approximately 0.5 p.u..

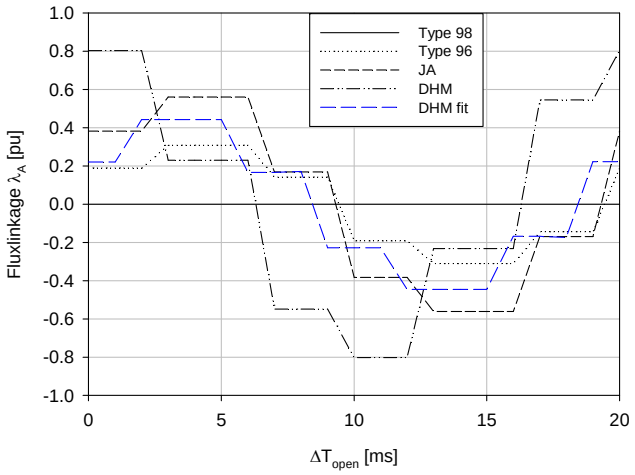

Fig. 9 Steady-state fluxlinkage after disconnection, phase A. Current interrupted at zero crossing.

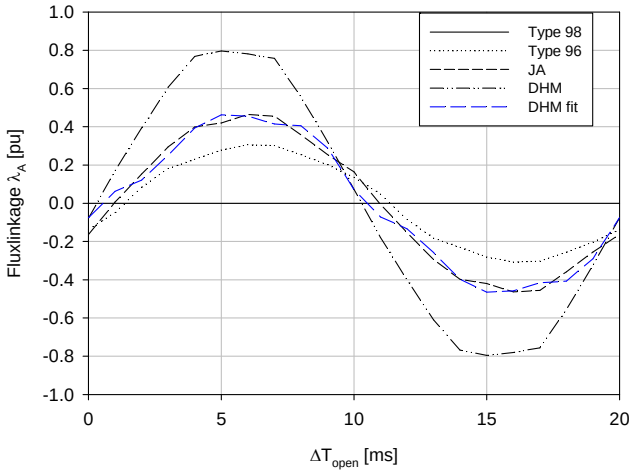

Fig. 10 Steady-state fluxlinkage after disconnection, phase A. Current chopped immediately at opening.

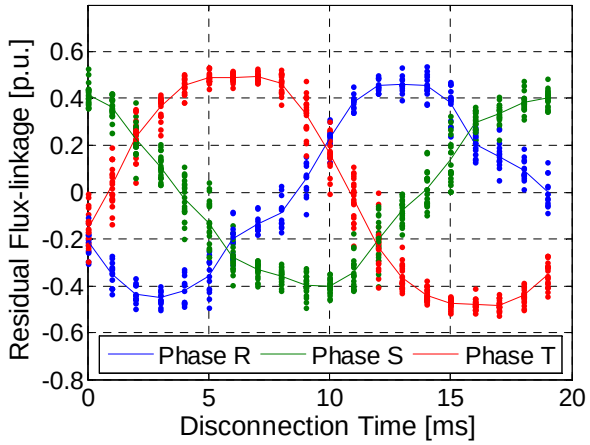

Fig. 11 Measured residual flux [15] as function of switching instance related to peak of phase T (ABC=RST). 20 different disconnections attempts (dots) per ms, and average value (solid line).

D. Inrush current shape test

In this section, the transformer model in Fig. 1 is energized from the HV side with rated excitation and zero source impedance. The transformer is ramped up to steady state and switched off 14 ms second after peak of phase A. The residual flux will then decay to a constant value in less than a second. Then the transformer is switched in at 3 ms after (prospective) peak voltage of phase This case is close to what gives the maximum negative inrush current in phase A. Fig. 12 shows the measured inrush current of the transformer [15]. Figures 13-16 show the simulated magnetization and inrush currents when switching the transformer on the HV side.

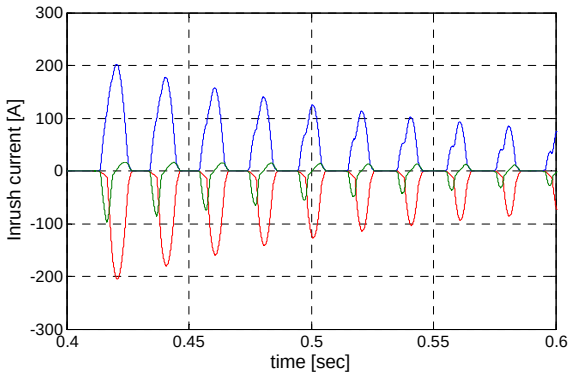

Fig. 12 Measured inrush current from [15]. Red, blue, green color or phase A, B, C, respectively.

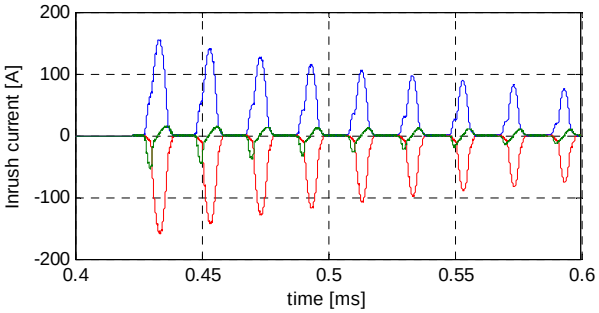

Fig. 13 Simulated HV side inrush currents of the transformer model of Fig. 1 with the Type 98 magnetization components.

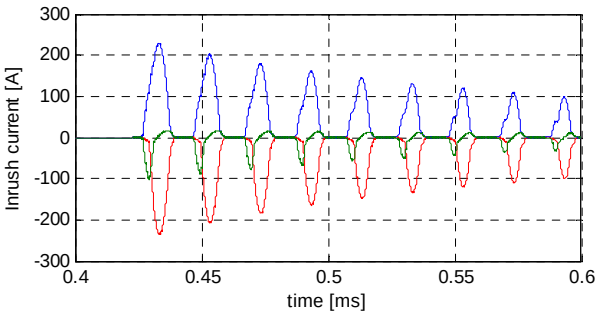

Fig. 14 Simulated HV side inrush currents of the transformer model of Fig. 1 with the Type 96 magnetization components.

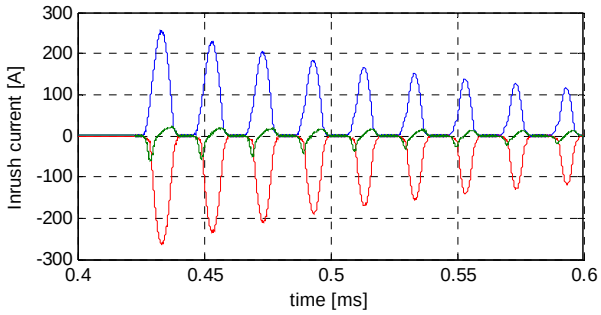

Fig. 15 Simulated HV side inrush currents of the transformer model of Fig. 1 with the JA magnetization components.

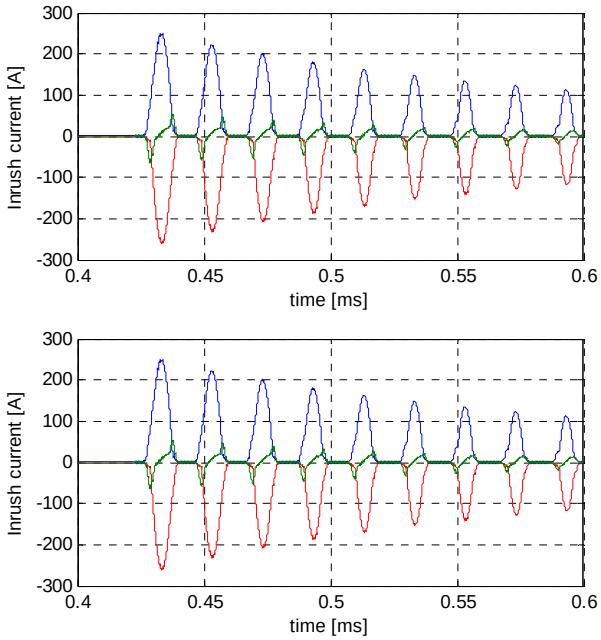

Fig. 16 Simulated HV inrush currents of the model of Fig. 1 with the basic (top) and fitted (bottom) DHM magnetization components.

E. Maximum inrush current tests

The peak inrush current test was performed by varying opening and closing times of the circuit breaker on the 11.43 kV side systematically with 1 ms resolution. Closing is performed ~0.3 sec after the opening when residual flux has decayed to a constant value. Δt_{open}=0 means opening at voltage peak and Δt_{close} = 0 means closing at the voltage peak. In each of the 400 (=20*20) tests the maximum inrush current peak is recorded. This test was also performed in the lab [16] with the result shown in Fig. 17.

Figures 18-22 show the maximum inrush current pattern obtained for the five magnetization models.

The maximum inrush current is determined by the leakage impedance and the final slope of the magnetization elements which here are the same, based on (1)-(2). The source impedance is zero in the simulations and unknown but small in the measurements. The residual flux pattern is also clearly reflected in the maximum inrush current. A high residual flux gives larger inrush current peaks as seen in Fig. 21 and a flatter diagonal path (Δt_{open}=Δt_{close}) as seen in Figures 20-22, and opposite in Fig. 19. Zero residual flux gives of course only closing time dependency as shown in Fig. 18. Fig. 23 shows the inrush current pattern for the DHM fitted model with the off-core inductance of the leg increased to L_{LC}=0.5·L_{HL}.

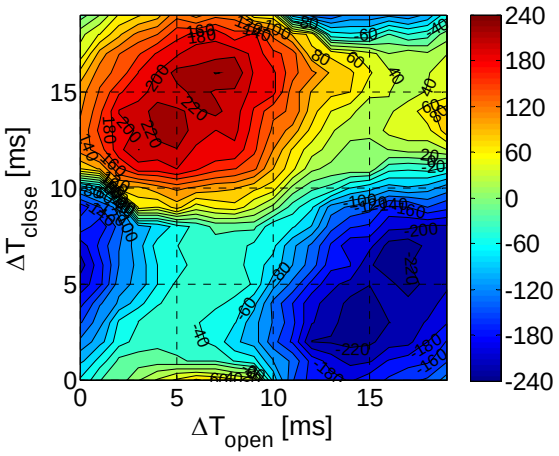

Fig. 17. Measured maximum inrush current as function of switching instances [16]. Max inrush 240 A.

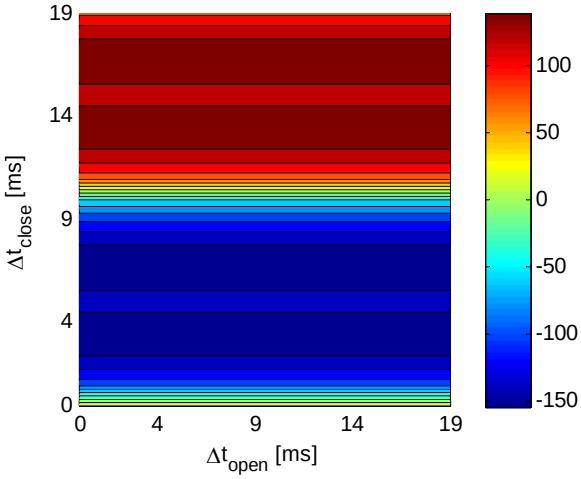

Fig. 18. Inrush current pattern Type 98. Max inrush 154.0 A.

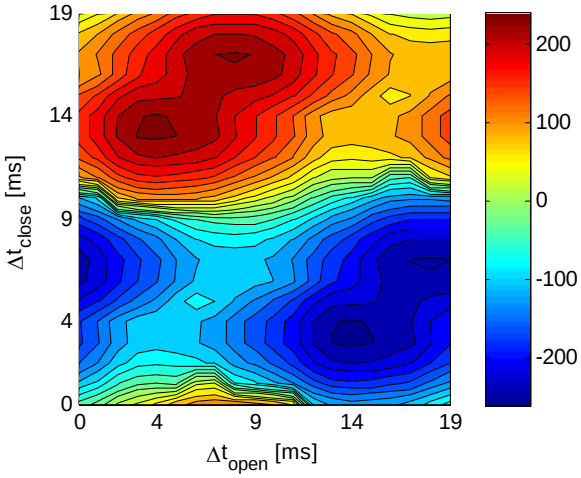

Fig. 19 Inrush current pattern Type 96. Max inrush 243.7 A

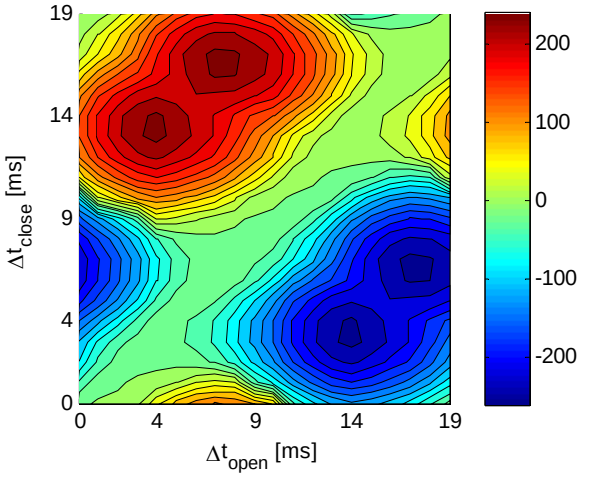

Fig. 20 Inrush current pattern JA. Max inrush is 246.1 A

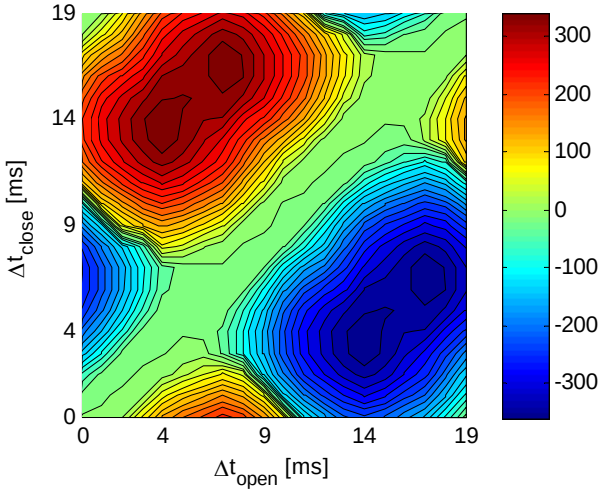

Fig. 21 Inrush current pattern DHM. Max inrush is 358.1 A

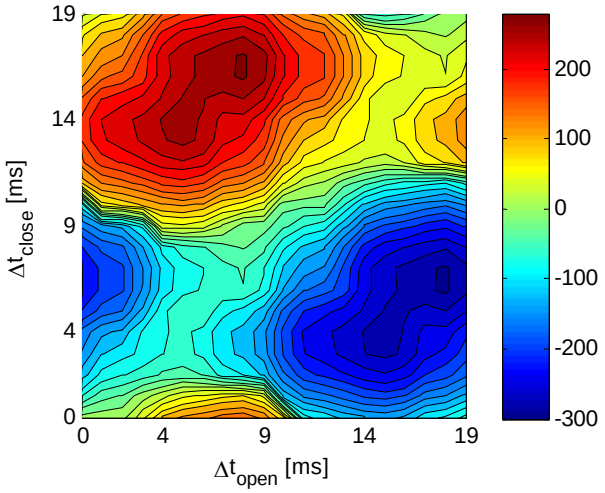

Fig. 22 Inrush current pattern DHM fit. Max inrush is 284.1 A.

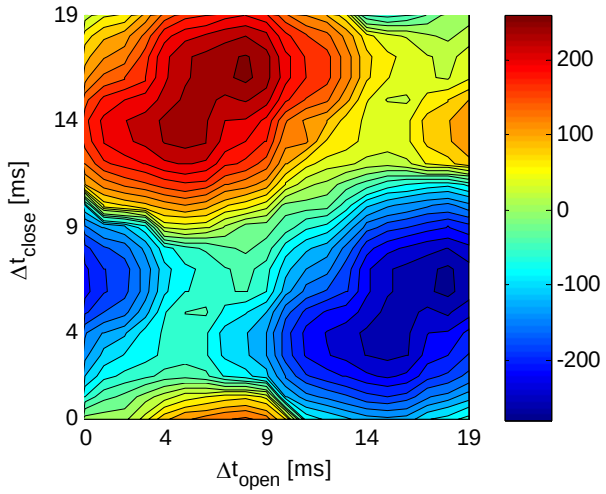

Fig. 23 Inrush current pattern DHM fit with L_{LC}=0.5·L_{HL}. Max inrush current is 265.1 A.

V. Discussion

All the investigated models are based on absolute core dimensions and the number of winding turns. In addition, the DHM model is based on selection of the core material (Armco steel M-5), while the other models are based on open circuit test report data. The DHM-fit model is, besides the test-report, also fitted to the maximum residual flux.

The JA (together with the fitted DHM) model gives the best residual flux estimation and the best inrush current representation. The model is also the most difficult to use and the parameter fitting is not standard or straight forward. The fitted DHM model gave the best core loss representation. The Type 98 and Type 96 components give the best rest report magnetization current representation as expected since they are fitted to these data by using the Hybrid Transformer implementation [3, 4]. The Type 96 model also gives somewhat reasonable agreement with residual flux and inrush current. This is probably due to the fact that the test report included samples high up in saturation and that the final slope of the magnetization curves could be calculated from design information (2). The DHM model is the easiest to use and requires only a few design input data. The model is in principle based on core-steel manufacturer's catalog data. Whether such magnetic data can be used in real transformer modeling with laminated and stacked cores is still discussable. Certainly core loss and stacking factor corrections are necessary and the core joints have to be taken into account somehow. This paper has shown that the DHM model produce results comparable to measurements when fitted to the available data.

The fact that some magnetization models show good results in this paper does not automatically mean they are correct for other type of tests, for instance with other source frequencies and harmonics. This applies in particular to the Type 98 component [8].

The transformer model in Fig. 1 is topologically correct but still quite simple. It is evident that the leakage model can have

a significant effect on inrush currents when the off-core flux paths become more important. The inrush current when the HV winding is excited is primarily influenced by the air-core inductance composed of the leakage inductance L_{HL}, the off-core inner inductance L_{LC} and the final slope of the magnetization inductance L_{∞}. Small changes can have a large effect. Using L_{LC}/L_{HL}=0.5 instead of 0.33 gives lower inrush currents as seen in Fig. 23. Here we have only included the off-core flux path effect in the inductance L_{LC} for the leg but a similar (but more difficult to obtain) effect exists also for the yokes and a more accurate zero sequence paths representation can be used [17]. Since also the source impedance is ignored in the inrush simulations it is expected that simulated inrush currents become higher than measured.

Accurate representation of the measured magnetization current shape was not achieved with the studied models. This is however not important for power system transient studies at least not at low excitations. A further analysis of this is beyond the scope of this paper.

That fact that the transformer had an isolated neutral where the inrush current tests were made introduced numerical challenges for the JA and DHM models that were solved by adding and tuning large resistors in the isolated HV neutral and at the open LV secondary.

Table II summarizes the magnetization model behavior.

TABLE III
BENCHMARK SUMMARY

Magn. Comp.	OC test report	Ring-down	Inrush
Type 98	Good Low P_0 at E0>rated	Zero	Too low. No pattern
Type 96	Good Low P_0 at E_0>rated	Low	OK Pattern different at diagonal
JA	Too low I_0 and P_0 at E_0> rated	OK	OK Pattern OK
DHM	Too low I_0 and P_0.	Too high	Too high; Pattern OK
DHM fit	Too low I_0 at E_0<rated; loss OK	OK	A bit too high; Pattern lacks two ±peaks and the flat diagonal

VI. CONCLUSION

The DHM model was recently implemented in ATP-EMTP. The model is a magnetic model based on manufacturer's core-steel catalog data. A real transformer with laminated and stacked cores is different, however. There are joints with air-gaps between yokes and legs and increased losses in these parts. It is thus not obvious that the basic DHM model is directly suitable for transformer studies. Fig. 3 shows that this model behaves different from the other models in this study. Applying core-loss, air-gap and stacking factor corrections is necessary to bring a transformer model based on such component sufficiently close to measurements. Further improvement of the DHM-based transformer model in its fitting to open circuit test data can be achieved by accounting for the deviation of the magnetic flux in the core laminations from the rolling direction in the T-joint areas.

VII. REFERENCES

[1] J. A. Martinez and B. A. Mork, "Transformer modeling for low- and mid-frequency transients – a review", *IEEE TPWRD*, vol. 20, no. 2, pp. 1625-1632, April 2005.

[2] J. A. Martinez (Ed), Power System Transients - Parameter determination, CRC Press, 2010.

[3] H. K. Høidalen, B. A. Mork, F. Gonzalez, D. Ishchenko, N. Chiesa: "Implementation and verification of the Hybrid Transformer model in ATPDraw", Electric Power Systems Research 79 (2009), 454-459.

[4] H. K. Høidalen, N. Chiesa, A. Avendaño, B. A. Mork, "Developments in the hybrid transformer model – Core modeling and optimization", IPST, Delft, the Netherlands June 14-17, 2011.

[5] V. Brandwajn, H. W. Donnel, I. I. Dommel, "Matrix representation of three-phase N-winding transformers for steady-state and transient studies", *IEEE TRPAS*, Vol. PAS-101, Issue: 6, 1982, pp. 1369 - 1378.

[6] Bonneville Power Administration: "EMTP Theory Book", Branch of System Engineering, Oregon, USA, 1987 (available at the secure website: http://www.eeug.org).

[7] Canadian/American EMTP User Group: "ATP Rule Book", Portland, Oregon/USA, revised and distributed by the EEUG Association, 2014

[8] N. Chiesa, H. K. Høidalen, "Hysteretic iron-core inductor for inrush current modeling in EMTP", 16th PSCC, Glasgow, UK, Jul. 2008.

[9] N. Chiesa, B.A. Mork, H. K. Høidalen, "Transformer model for inrush calculations: Simulation, measurements and sensitivity analysis", *IEEE TPWRD*, vol. 5, pp. 2599-2608, Oct. 2010.

[10] N. Chiesa, "Power transformer modeling for inrush current calculation," Doctoral theses, NTNU, 2010.

[11] S. E. Zirka, Y. I. Moroz, R. G. Harrison, N. Chiesa, "Inverse hysteresis models for transient simulation", *IEEE TPWRD*, vol. 29, pp. 552-559, 2014.

[12] S. E. Zirka, Y. I Moroz, P. Marketos, A. J. Moses, D. C Jiles, and T. Matsuo, "Generalization of the classical method for calculating dynamic hysteresis loops in grain-oriented electrical steels", *IEEE TRMAG*, vol. 44, pp. 2113-2126, 2008.

[13] S. E. Zirka, Y. I Moroz, N. Chiesa, R.G. Harrison, and H. K. Høidalen, "Implementation of inverse hysteresis model into EMTP – Part II: Dynamic model," *IEEE Trans. Power Delivery*, accepted for publication.

[14] G. Bertotti, *Hysteresis in Magnetism*. San Diego, CA: Academic, 1998.

[15] N. Chiesa, H. K. Høidalen, "Systematic switching study of transformer inrush currents - simulations and measurements", IPST'09, Kyoto.

[16] N. Chiesa, H. K. Høidalen, "Novel approach for reducing transformer inrush currents. Laboratory measurements, analytical interpretation and simulation studies", *IEEE TPWRD* vol. 25, no. 4, pp. 2609-2616, 2010.

[17] S. E. Zirka, Y. I Moroz, and C. M. Arturi, "Accounting for the influence of the tank walls in the zero-sequence topological model of a three-phase, three-limb transformer," *IEEE TPWRD*, vol. 29, no. 5, pp. 2172-2179, Oct. 2014.